Scientific Research Publishing

Engineering, 2025, 17(6), 315-334
https://www.scirp.org/journal/eng
ISSN Online: 1947-394X
ISSN Print: 1947-3931

CFD Analysis for a Screw Heat Sink Absorber Tube of a Solar Water Heater Collector

Gulom Uzakov*, Sokhiba Shamurotova, Bobir Toshmamatov, Khayrulla Davlonov

Department of the "Power Engineering", Karshi State Technical University, Karshi, Uzbekistan
Email: *bobur160189@mail.ru

How to cite this paper: Uzakov, G., Shamurotova, S., Toshmamatov, B. and Davlonov, K. (2025) CFD Analysis for a Screw Heat Sink Absorber Tube of a Solar Water Heater Collector. *Engineering*, **17**, 315-334.
https://doi.org/10.4236/eng.2025.176019

Received: April 29, 2025
Accepted: June 23, 2025
Published: June 26, 2025

Abstract

This study investigates and compares the computational fluid dynamics (CFD) analysis of smooth absorber finned tubes and helical fin absorber tubes used in solar water heating collectors. The three-dimensional numerical simulations were conducted using COMSOL Multiphysics software to analyze fluid flow and heat transfer characteristics. The research is structured into three main sections. In the first section, absorber finned tubes made from different materials, including stainless steel, iron, copper, and aluminum, are evaluated to determine their impact on thermal performance. The second section focuses on the comparative analysis of two different geometric configurations of absorber finned tubes, assessing their influence on heat transfer efficiency. The final section investigates the performance of a selected absorber tube—identified as optimal from the previous analysis—by introducing internal helical fins with varying pitch sizes of 25 mm, 50 mm, 75 mm, and 100 mm. The influence of these internal fins on heat transfer enhancement and flow characteristics is systematically examined. The findings of this study provide valuable insights into the optimization of absorber tube designs for solar water heating systems, contributing to improving efficiency and performance in thermal energy applications.

Keywords

Solar Energy, Solar Water Heater Collector, Numerical Simulation, Absorber Tube

1. Introduction

Solar energy can meet the energy needs of the world using a few percent of uninhabited areas [1]. The improvement of solar energy devices is developing rapidly. Heat exchangers, which transfer thermal energy through direct and indirect contact between fluids, are considered an indispensable part of several industries, from

pharmaceuticals to petrochemicals. Indirect contact heat exchangers are extensively used in solar systems. Due to the increasing importance of solar energy, nowadays, improving the performance of solar systems is one of the most important challenges for human beings and researchers [2]. One of the most effective types of solar water heating collectors are vacuum collectors, but they are expensive. Therefore, it is desirable to increase the efficiency of flat solar water heater collectors. Recently, many efforts have been made by scientists to increase the efficiency of this type of collector. Actually, the SWHC component is a heat exchanger in which heat transfer fluid (HTF) flows in the receiver tube and absorbs the radiated solar energy. In order to improve the thermal performance of this type of heat exchanger, various methods have been proposed and studied by researchers. Table 1 explores and presents this information to some extent.

Table 1. Overview of articles to improve the heat transfer.

Author	Year	Method (Exp/Num)	Inserts	Results
Zaboli *et al.* [2]	2021	Numerical	In the present work, a parabolic trough solar collector (PTC) with inner helical axial fins as swirl generator or turbulator is considered and analyzed numerically [2]	Results show that the thermal performance improvement by 23.1% could be achieved by using one of the proposed innovative parabolic trough solar collectors compared to the simple one [2]
Pambudi *et al.* [3]	2023	Experimental	In this research, a novel configuration for solar water heating (SWH) was proposed, featuring a v-corrugated collector made by adding an aluminum foil foam insulation with a 5 mm thick plywood base [3]	The experimental results indicated that the highest energy efficiency (50%) was achieved at a flow rate of 240 Lph, followed by 40% and 34% for 180 Lph and 120 Lph, respectively [3]
Aramesh *et al.* [4]	2023	Experimental	The present study proposes a novel built-in PCM-based storage design as an alternative to the bulky hot water storage tanks that residential solar water heaters are conventionally equipped with [4]	At the end of the experiment, the overall thermal efficiency of the normal and self-storing collectors are 49% and 72%, respectively [4]
Rahi *et al.* [5]	2021	Experimental and Numerical	This work includes theoretical, numerical, and experimental investigation of using spiral solar collector [5]	1) Increasing the water flow in the spiral pipe from (0.03125 - 0.0625) lit/sec leads to increased thermal efficiency of about 15%. 2) Increasing in tube diameter also leads to an increase in water outlet temperature. 3) Central water inlet with the full flow rate has been achieved the optimum efficiency of 82.5% [5]
Yehualashet *et al.* [6]	2022	Experimental and Numerical	In this research work, an attempt has been made to experimentally and numerically analyze a newly designed corrugated plate solar collector characterized by its chevron corrugated (sinusoidally profiled) absorber surface and thereby improved the thermal contact [6]	A maximum collector outlet temperature and collector efficiency differences of 7:43˚C and 7:03% was achieved both of which increased with amount of insolation [6]
Barbosa *et al.* [7]	2019	Experimental	Two low-cost solar water heaters are offered [7]	The collectors presented maximum efficiencies and global heat transfer coefficients of 40.9% and 2.69 W $^{\circ}C^{-1}$ for tube pattern arranged in parallel (LCSHP), and 37.8%, and 3.07 W $^{\circ}C^{-1}$ for the one arranged in series (LCSHS) [7]

Continued

Syahruddin *et al.* [8]	2021	Experimental and Numerical	The thermal performance of a solar water heater system using absorber plate with phase change material (PCM) as thermal energy storage is presented in this study [8]	The results showed that the average collector efficiency between absorber plate with and without PCM storage is 70.98 % using experimental study and 67.73 % using numerical simulation study [8]
Sadhishkumar *et al.* [9]	2014	A review	This paper discusses optimization and simulation methods of solar water heating systems to understand the flow and heat behavior in solar collectors leading to improved thermal performance of SWH collectors [9]	The enhancement of heat transfer in the solar collector with twisted tape is found to be better than the conventional plain tube collector [9]
Farahani *et al.* [10]	2021	Numerical	In this paper, the application of using a phase change material (PCM) and a porous material for thermal performance of a solar water heater (SWH) based on a cylindrical solar collector, which is cut from the oblique surface, is comprehensively studied [10]	The maximum thermal efficiency ratio occurs at a thickness of 70 mm, 40 mm, and diameter of 150 mm for cases 1, 2, and 3, respectively, with corresponding efficiencies of 116%, 109.7%, and 110.41% [10]
Alwan *et al.* [11]	2022	Experimental and Numerical	The thermal performance of the SWH was predicted using Fortran 90 programming language. SWH was designed as a square shape with dimensions of 110 cm length, 120 cm width and 10 cm depth and tested by integrating with a modified solar distiller to increase the water temperature in the basin at a constant mass flow rate of 1.2 l/min [11]	During the four typical days of the experiment, the highest water temperatures of the solar collector were recorded during midday, *i.e.* 57.2˚C, 64.4˚C, 52.4˚C and 49˚C at the inlet, and 62.8˚C, 71˚C, 57.4˚C and 53.2˚C at the outlet for 19 June, 17 July, 22 August and 15 September 2019, respectively, while the solar radiation intensities recorded are 957, 1022, 840 and 723 W/m^2 for the test days [11]
Ramasamy *et al.* [12]	2015	Experimental	The main objective of the experiment is to maintain the velocity at the outlet and the better outlet water temperature by selecting the correct shape and measurement of fins [12]	We have implemented the circular fins and rectangular fins among which the circular fins have more efficiency than that of rectangular fins. Normally the found temperature difference between the solar water heater with fins and without fins is (7 - 8) degree Celsius in normal conditions [12]
Bhowmik *et al.* [13]	2017	Experimental	The solar reflector used here with the solar collector to increase the reflectivity of the collector [13]	A prototype of a solar water heating system was constructed and obtained the improvement of the collector efficiency around 10% by using the reflector [13]
Darbari *et al.* [14]	2021	Numerical	In this study, a numerical simulation is carried out to investigate the thermal efficiency of the flat plate thermosyphon solar water heater with different nanofluids [14]	As the volume fraction of nanoparticles increases, the mean temperature of absorber decreases. As the ambient temperature increases from 20˚C to 40˚C, the efficiency increases by 5.5%. As the inlet temperature of water increases from 30˚C to 55˚C, the efficiency decreases by 15% [14]

Modern solar water heating collectors (SWHCs) can achieve higher thermal efficiency compared to conventional flat-plate or vacuum tube collectors, especially when integrated with phase change materials (PCMs) or advanced heat retention systems. However, these high-efficiency systems come with a significant cost, making them less accessible to economically disadvantaged populations. The price of advanced SWHCs ranges between $248 and $1200, with additional expenses for transportation, installation, and maintenance, sometimes reaching an average of $3600 [9]-[11]. These high costs make it difficult for people in low-income communities

to afford such technologies, despite their potential benefits in reducing dependence on conventional energy sources.

According to the latest global poverty statistics, approximately 9.2% of the world's population (around 700 million people) live in extreme poverty, surviving on less than $1.90 per day. A vast majority—around 90% of these individuals—reside in Sub-Saharan Africa and South Asia, regions that experience high solar radiation levels throughout the year [12]. Ironically, these are the very areas where solar water heating systems could provide the most benefits, reducing the reliance on expensive and often unreliable electricity or fossil fuel-based heating methods [15]-[18].

Given the economic constraints faced by such populations, there is an urgent need to develop solar water heating systems that are not only thermally efficient but also cost-effective and easy to manufacture, transport, install, and maintain. Traditional flat-plate solar collectors are among the most affordable solutions available today. However, their efficiency is often lower compared to vacuum tubes or concentrated solar collectors. To bridge this efficiency gap while keeping costs low, modifications and optimizations in flat-plate collector designs can be explored.

Improving Flat-Plate Solar Water Heating Collectors

To make flat-plate collectors a more viable solution for low-income regions, several design optimizations can be implemented:

Enhanced Absorber Materials: Utilizing cost-effective yet high-conductivity materials such as aluminum with selective coatings can improve heat absorption while maintaining affordability.

Incorporation of Phase Change Materials (PCMs): Integrating low-cost PCMs into the collector system can significantly increase heat retention, allowing for hot water availability even after sunset.

Reflector Integration: Adding reflectors to direct more solar radiation onto the absorber surface can enhance energy capture without significantly increasing costs.

Optimized Fluid Flow Design: Implementing helical or finned absorber tubes within the collector can enhance heat transfer efficiency, reducing thermal losses and improving performance.

Use of Locally Available Materials: By designing collectors that can be manufactured with materials readily available in developing countries, costs can be reduced, and local economies can be stimulated.

Modular and Scalable Design: Developing modular systems that can be expanded based on energy demand allows households to invest in smaller systems and gradually upgrade as their financial capacity improves.

By focusing on these improvements, flat-plate solar water heating collectors can be transformed into highly efficient yet affordable solutions, making solar thermal technology more accessible to the world's poorest communities.

This paper focuses on improving the optimized design of fluid flow, and investigates how implementing spiral or finned absorber tubes inside the collector can improve heat transfer efficiency, reduce thermal losses, and improve performance.

2. Materials and Methods

Flat plate solar water heater (SWH) collectors are primarily utilized in the systems illustrated in Figure 1(a), while Figure 1(b) presents the visual representation of an SWH flat plate collector. Furthermore, Figure 1(c) depicts the geometric configuration of the absorber finned tube of the investigated SWH flat plate collector. Additionally, Table 2 provides the geometric constants and physical parameters relevant to the study. According to the conducted investigation, the flow within the tube is turbulent. Three-dimensional numerical simulations were performed using COMSOL Multiphysics software, employing the Turbulent Flow and Heat Transfer in Solids and Fluids physics interfaces. The finite element method (FEM) was selected as the solution approach. Water at an inlet temperature of 20˚C was introduced into the tube at varying velocities, specifically 0.01, 0.02, 0.025, and 0.035 $m \cdot s^{-1}$. The velocity-inlet and pressure-outlet boundary conditions were applied at the inlet and outlet ports, respectively. In the first stage of the investigation, a heat flux of 1000 W/m^2 was applied to the surface of the SWH flat plate. Moreover, the thermophysical properties of the tube material and the working fluid are provided in Table 3.

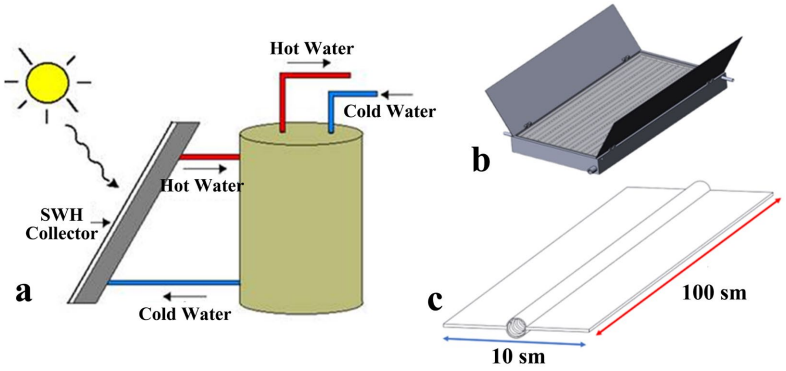

Figure 1. (a) SWH system; (b) SWH collector; (c) Absorber finned tube.

Table 2. Physical parameters of the analyzed absorber tube for SWH collector.

Parameters		Value
Diameter of the inner tube	D_1	8 mm
Diameter of the outer tube	D_2	10 mm
Length of the tube	L	750 mm
Height of the fins	H	2 mm
Thickness of the fins	th	2 mm
Helix pitch of the fins	P	10, 15, 20, 25 mm
Helical angle of the fins	α	180˚
Length of the wings	l	35 mm
Inlet velocity	u	0.01, 0.02, 0.025, 0.035 $m \cdot s^{-1}$
Solar radiation	I	1000 $W \cdot m^{-2}$

Table 3. The thermo-physical properties of materials.

Fluid	Pipe				Property
Water	Steel AISI 4340	Iron	Aluminum	Copper	
4182	475	440	900	385	Heat capacity at constant pressure [J/(kg·K)]
997 (at 25˚C)	7850	7870	2700	8960	Density [kg/m^3]
0.606	44.5	76.2	237	400	Thermal conductivity [W/(m·K)]
~4.3 × 10^{-4} (at 25˚C)	12.3e−6	12.2e−6	23 × 10^{-6}	17e−6	Coefficient of thermal expansion [1/K]
~1.01 (for water vapor at 100˚C)	0.48	0.45	~1.67 (for monatomic metals)	0.39	Ratio of specific heats [kJ/(kg·K)]

This study consists of two main sections. The first section investigates a finless heat-absorbing tube made from four different materials. Numerical simulations were conducted for Steel AISI 4340, Iron, Aluminum, and Copper at varying flow velocities, as presented in Table 3. Based on the obtained results, the most optimal material was selected. The second section focuses on the analysis of four different geometries incorporating internal spiral fins within the absorber tube. The obtained results are compared with a conventional collector that lacks any additional fins. The schematic representation of the evaluated geometry from the first section is illustrated in Figure 2. Figure 3 provides a visualization of the internal spiral fins inside the absorber tube, along with the selected mesh configuration. The details regarding the mesh structure are summarized in Table 4. In the second section, the performance of the internal spiral-finned receiver tube (P) is analyzed based on the material selected in the first section. Various step sizes of the internal fins, specifically 10 mm, 15 mm, 20 mm, and 25 mm, are examined. The evaluated cases and corresponding geometries are depicted in Figure 4.

Finite Element Analysis

The three-dimensional Navier Stokes equation with energy equation was solved using the finite element technique COMSOL Multiphysics. The flow is incompressible and steady state. The water is a circulating fluid with inlet velocities u_1 = 0.01 m/s, u_2 = 0.02 m/s, u_3 = 0.025 m/s, u_4 = 0.035 m/s and inlet temperature 25˚C. The formula and boundary conditions and geometry used for this model can be found in Table 2 and Table 3. Figure 2 shows Model 1 and Figure 3 shows Model 2, while the FEM model is also presented, with the number of elements detailed in Table 4. The inlet temperature is set to T_{in} and is equal to 25˚C. The ambient temperature is also 25˚C. The solar radiation (heat flux) on the absorber fin surface and tube is set to I_0 = 1000 W/m^2. The inlet velocity for the water flow was chosen to be 0.01 m/s, 0.02 m/s, 0.025 m/s, and 0.035 m/s.

At the outlet of the absorber tube, a zero-voltage state is maintained, which ensures the neutralization of the potential difference at the outlet. In addition, the boundary surfaces of the environment are not insulated, which does not prevent heat loss to the external environment. This approximates the results obtained in

real conditions. For this model, a 3D model was created based on the dimensions and data given in Table 1, a mesh consisting of elements of various sizes and types was created to ensure the correct representation of the geometry, and an analysis of the described mesh was performed.

Table 4. Finite elements used in the calculation.

Elements type	Domain elements	Boundary elements	Edge elements
Number of elements (M1)	258,569	20,172	658
Number of elements (M2)			

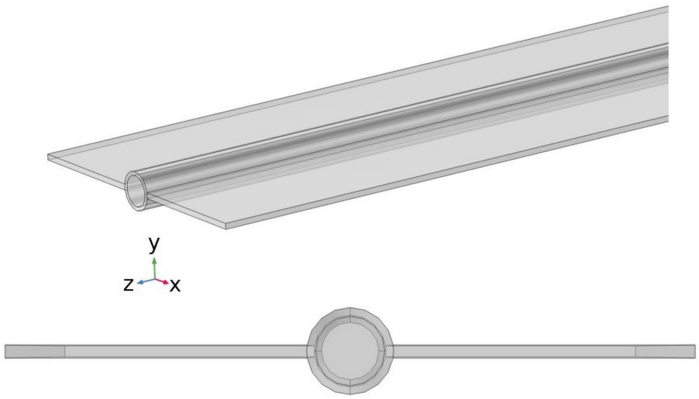

Figure 2. Absorber finned tube (Model 1).

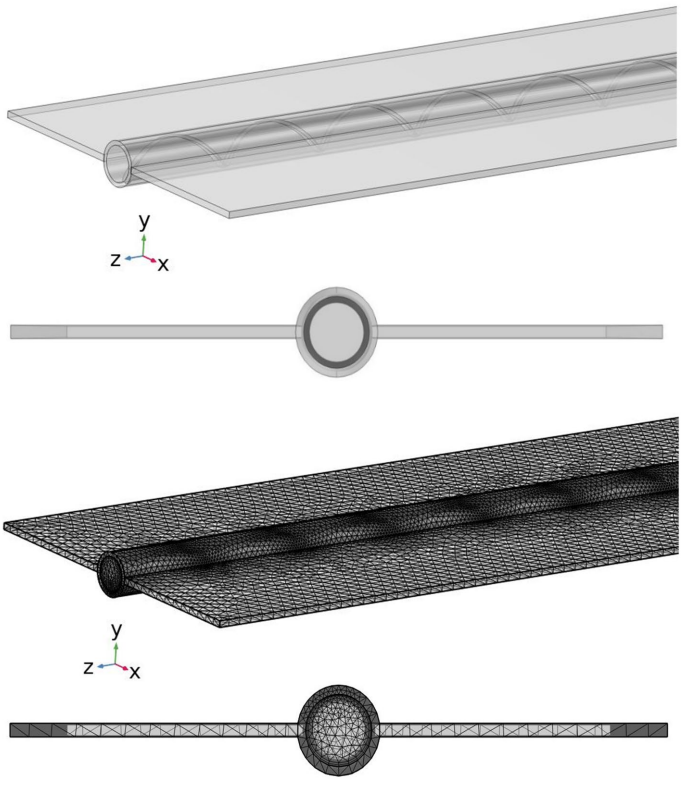

Figure 3. Absorber finned tube and Finite element model absorber finned tube (Model 2).

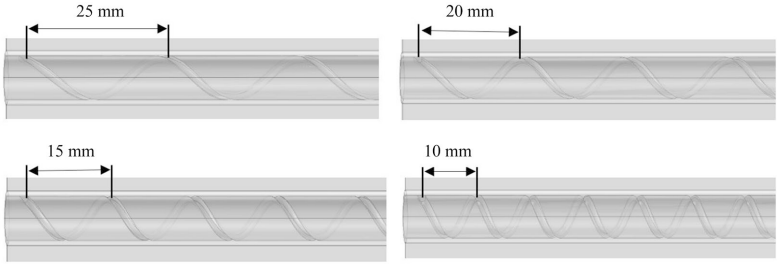

Figure 4. Various twisted channel absorber finned tube.

3. Governing Equations and Dimensionless Parameters

3.1. For Heat Transfer in Solids

The following equation is utilized for solving the Heat Transfer in Solids Interface.

$$\rho C_p\left(\frac{\partial T}{\partial t}+\boldsymbol{u}_{trans}\cdot\nabla T\right)+\nabla\cdot\left(\boldsymbol{q}+\boldsymbol{q}_r\right)=-\alpha T:\frac{dS}{dt}+Q \tag{1}$$

where, ρ is the density (kg/m^3), C_p is the specific heat capacity at constant stress (J/(kg·K)), T is the absolute temperature (K), $\boldsymbol{u}_{trans}$ is the velocity vector of translational motion (m/s), $\boldsymbol{q}$ is the heat flux by conduction (W/m^2), $\boldsymbol{q}_r$ is the heat flux by radiation (W/m^2), α is the coefficient of thermal expansion (1/K), S is the second Piola-Kirchhoff stress tensor (Pa), Q contains additional heat sources (W/m^3).

For a steady-state problem, the temperature does not change with time and the terms with time derivatives disappear.

The first term on the right-hand side of Equation (1) is the thermoelastic damping and accounts for thermoelastic effects in solids:

$$Q_{ted}=-\alpha T:\frac{dS}{dt} \tag{2}$$

It should be noted that the d/dt operator is the material derivative, as described in the Time Derivative subsection of Material and Spatial Frames.

3.2. For Heat Transfer in Fluids

The Heat Transfer in Fluids Interface solves for the following equation ((2)-(5) in Ref. [5]):

$$\rho Cp\left(\frac{\partial T}{\partial t}u\cdot\nabla T\right)+\nabla\cdot\left(q+q_r\right)=\alpha_p T\left(\frac{dp}{dt}+u\cdot\nabla_p\right)+\tau:\nabla u+Q \tag{3}$$

which is derived from Equations (4)-(13), considering that:

The following equations describe the heat transfer and efficiency of a solar water heater (SWH):

Cauchy stress tensor:

$$\sigma=-pI+\tau \tag{4}$$

where, σ is the stress tensor, p is the pressure, I is the identity tensor, and τ is the viscous stress tensor. This equation represents the distribution of forces in fluid mechanics.

Thermal expansion coefficient:

$$\alpha_P = \frac{1\partial\rho}{\rho\partial T} \tag{5}$$

where, α_P is the thermal expansion coefficient, ρ is the density, and T is the temperature. This equation describes the dependence of density on temperature.

Heat changes due to pressure:

$$Q_P = \alpha_P T\left(\frac{dp}{dt} + u\cdot\nabla_p\right) \tag{6}$$

where, Q_P is the heat exchange due to pressure effects, u is the velocity vector, and ∇_p is the pressure gradient. This equation characterizes the influence of pressure and temperature variations on heat transfer.

Viscous dissipation heat flux:

$$Q_{vd} = \tau : \nabla u \tag{7}$$

where, Q_{vd} is the heat generated due to viscous dissipation, and ∇u is the velocity gradient. This equation accounts for heat energy generated due to viscous effects.

Total solar heat energy:

$$Q_{solar} = Q_{fluid} + Q_{absorber} + Q_{rad} \tag{8}$$

where, Q_{solar} is the total incoming solar energy, Q_{fluid} is the heat transferred to the fluid, $Q_{absorber}$ is the heat absorbed by the absorber, and Q_{rad} is the heat lost through radiation.

Heat transferred to the fluid:

$$Q_{fluid} = \dot{m}C_p\left(T_{out} - T_{in}\right) \quad [W] \tag{9}$$

where, $\dot{m}$ is the mass flow rate, C_p is the specific heat capacity of the fluid, T_{out} is the outlet temperature, and T_{in} is the inlet temperature. This equation determines the amount of heat transferred to the fluid.

Heat absorbed by the absorber:

$$Q_{absorber} = Q_{convective} + Q_{conductive} \quad [W] \tag{10}$$

where, $Q_{absorber}$ is the heat transferred via convection, and $Q_{convective}$ is the heat transferred via conduction.

Radiative heat loss:

$$Q_{rad} = \sigma\cdot\left(T_2^4 - T_{sky}^4\right) \quad [W] \tag{11}$$

where, σ is the Stefan-Boltzmann constant, T_2 is the absorber surface temperature, and T_{sky} is the sky temperature. This equation quantifies the amount of heat lost due to radiation.

Thermal efficiency:

$$\eta = \frac{Q_{fluid}}{Q_{solar}} = \frac{\dot{m}C_p\left(T_{out} - T_{in}\right)}{Q_{solar}} \tag{12}$$

where, η is the overall thermal efficiency of the system. This equation shows how

much of the incoming solar heat energy is effectively transferred to the working fluid.

These equations are essential for understanding the heat transfer processes in a solar water heater (SWH) and help improve system efficiency while minimizing heat losses.

4. Results

4.1. Model Validation

The developed Model 1 was compared with the experimental and simulation results presented in the study by Farhan *et al.* [19]. The geometric dimensions of Model 1 were adjusted to match those reported in [19], and boundary conditions for the simulation were set using input parameters such as inlet temperature, ambient temperature, and global radiation values at a specific time, ensuring consistency with the corresponding mass flow rate. According to [19], the experiment was conducted in Jamshedpur from 9:00 AM to 3:00 PM during April and May 2022. Experimental data for a mass flow rate of 0.5 L/min were obtained from the study by Farhan *et al.* The maximum recorded solar irradiance for the test day at 0.5 L/min was 824 W/m^2, with a peak temperature rise of approximately 6˚C at noon [19]. Experimental data were also recorded for a flow rate of 1 L/min, where the maximum solar irradiance on the test day reached 832 W/m^2, and the maximum temperature rise was 3.5˚C.

For all experimental tests, the maximum variation in steady-state data for inlet, outlet, and ambient temperatures was 1.1 K, 0.9 K, and 1.2 K, respectively, while the maximum difference in global radiation values during a single test was 48 W/m^2. These variations fall within the range defined by ASHRAE for experimental data [19] (**Figure 5**).

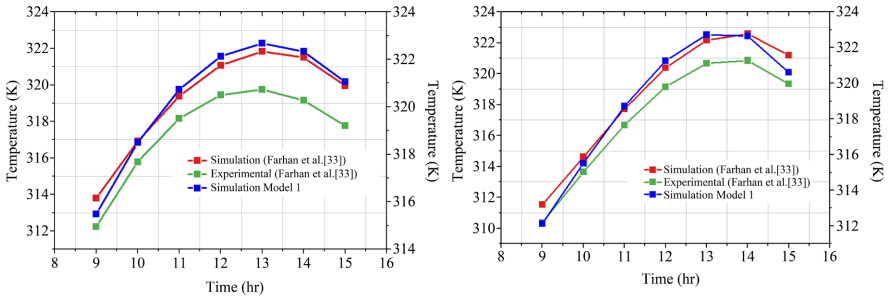

Figure 5. Validation simulation Model 1 with Farhan *et al.* absorber fins temperature (a), and water outlet temperature (b).

To compare these results, data from [19] were obtained (**Table 5**) and reprocessed. The reprocessing was carried out using the polynomial regression method, and the obtained results are presented in **Table 6**. For each derived result, the determination coefficient was calculated during the development of the polynomial regression equation (**Table 6**).

Table 5. Results for Farhan *et al.* and Model 1.

		0.5 lit/min			1 lit/min		
		9^{00}	12^{00}	15^{00}	9^{00}	12^{00}	15^{00}
Farhan *et al.* [19]	Simulation	313.8 K	321.1 K	320.0 K	311.6 K	320.5 K	321.2 K
	Experimental	312.2 K	319.5 K	317.8 K	310.4 K	319.2 K	319.2 K
Model 1	Simulation	315.5 K	322.1 K	321.1 K	312.2 K	321.3 K	320.7 K

Table 6. Polynomial regression equations and the values of the coefficient of determination based on them.

		$T = A + B \cdot \tau + C \cdot \tau^2 + D \cdot \tau^3$				
	0.5 lit/min	A	B	C	D	R^2
Farhan *et al.* [19]	Simulation	281.175	1.891	0.4123	−0.0244	0.9984
	Experimental	211.829	19.423	−1.06	0.0157	0.98407
Model 1	Simulation	258.98	8.68	0.2128	−0.006	0.99946
	1 lit/min	A	B	C	D	R^2
Farhan *et al.* [19]	Simulation	360.92	−20.11	2.315	0.07674	0.9922
	Experimental	333.82	−13.515	1.776	−0.06261	0.9811
Model 1	Simulation	345.8481	−16.84	2.12	−0.074	0.99717

To evaluate the reliability of the numerical model, the standard root means square error (RMSE) and mean absolute error (MAE) were used to evaluate the degree of agreement between the modeled and measured values. The lower the RMSE and MAE values, the higher the accuracy of the numerical model. They can be expressed as follows:

$$RMSE = \sqrt{\frac{\sum_{i=1}^{n}\left(P_i - O_i\right)^2}{n}} \tag{13}$$

$$MAE = \frac{\sum_{i=1}^{n}\left|P_i - O_i\right|}{n} \tag{14}$$

where, P_i is the measured value, O_i is the simulated value, and n is the number of measured values.

Table 7. Root means square error and mean absolute error.

	RMSE [K]	*MAE* [K]
Farhan *et al.* (simulation) and Model 1 for 0.5 lit/min	1.304	1.27
Farhan *et al.* (experimental) and Model 1 for 0.5 lit/min	2.85	2.73
Farhan *et al.* (simulation) and Model 1 for 1 lit/min	1.07	0.97
Farhan *et al.* (experimental) and Model 1 for 1 lit/min	1.50	1.47

The numerical model predicts the outlet temperature and compares the numerical results with the data obtained from experiments. The discrepancy between the

experimental and numerical results from [19] and Model 1 is illustrated in Figure 5 (Table 7)

4.2. Effect of Different Materials Tested on the Outlet Temperature of Water in the SWH Collector

In this section, the thermal efficiency of various materials is numerically investigated. Four different materials were considered, and the obtained results were compared. The analysis was conducted exclusively on Model 1 at different flow rates, as illustrated in Figure 2. The thermophysical properties of these materials and water are presented in Table 3, while the geometric dimensions and physical parameters of Model 1 are provided in Table 2.

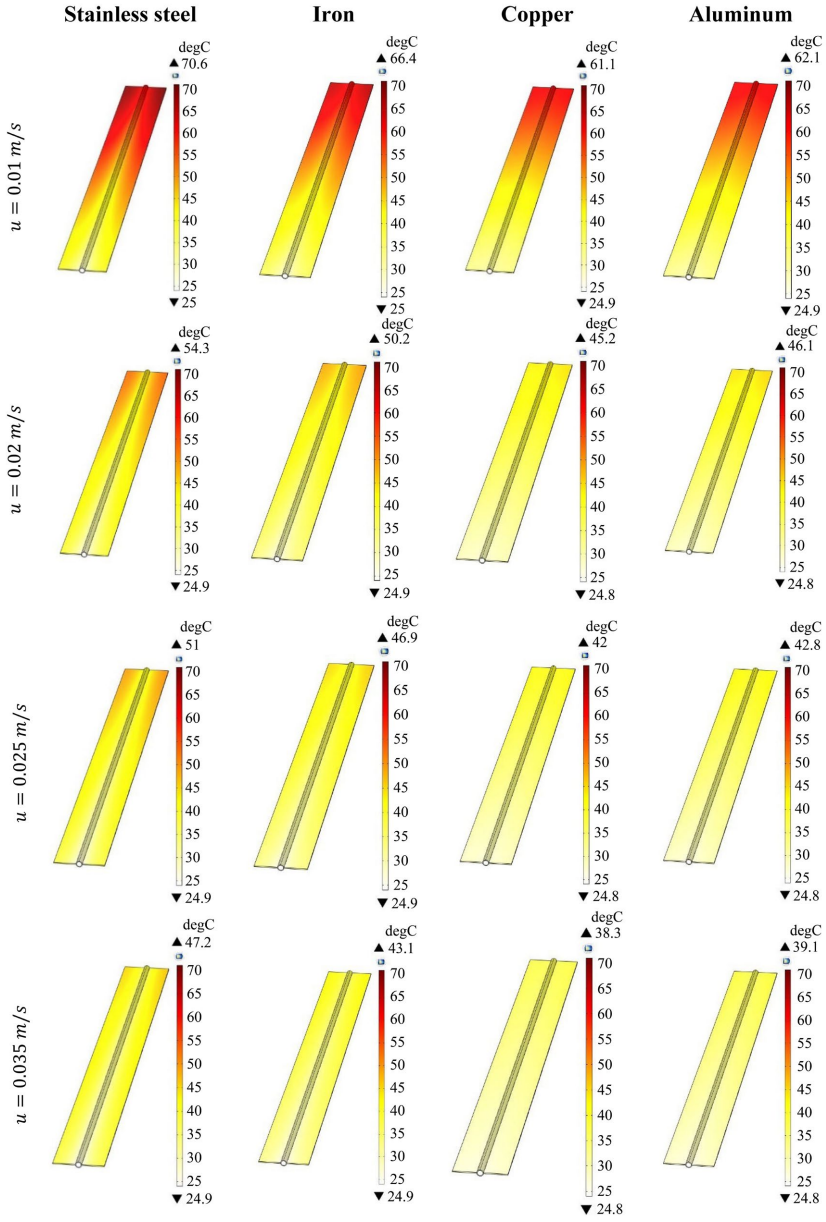

Figure 6. Surface temperatures of receiver tubes with different materials.

The results indicate that among the examined materials—Steel, Iron, Copper, and Aluminum, the surface temperature of copper was found to be the lowest (Figure 6). Additionally, the outlet water temperature in the Copper-based system was higher compared to other materials (Figure 7 and Figure 8). The inlet and outlet water velocities at different flow rates are depicted in Figure 9 and Figure 10.

Figure 7 shows the variation of the heat transfer fluid (HTF) temperature in a solar water heater (SWH) collector along the length of the collector. The study was conducted by comparing collector pipes made of different materials for a fluid moving at a speed of 0.01 and 0.02 m/s.

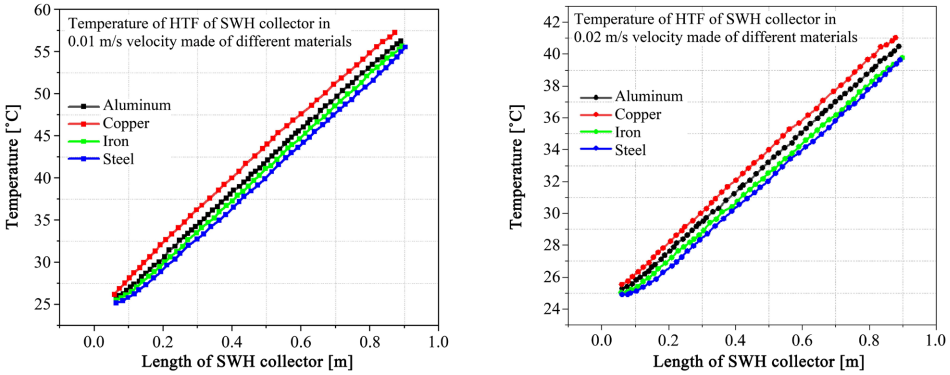

Figure 7. Temperature of HTF of SWH collector in 0.01 m/s and 0.02 m/s velocity made of different materials.

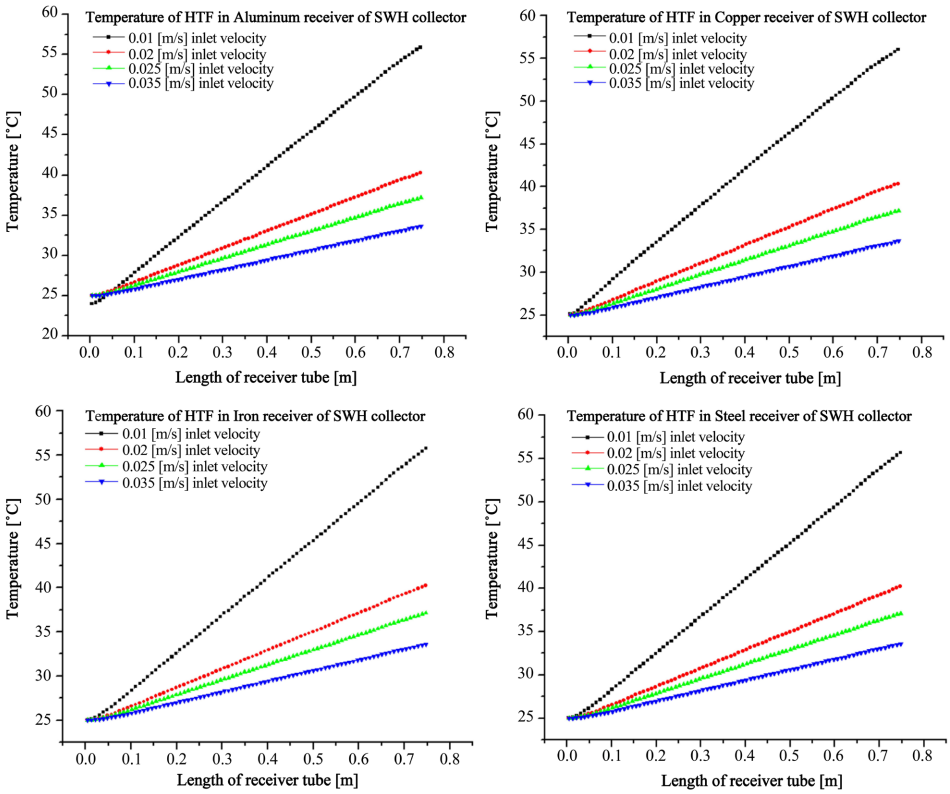

Figure 8. Temperature variation of HTF with the length of receiver made of various materials.

The results of Figure 7 show that the HTF temperature increases steadily with increasing collector length. However, the intensity of the temperature increase differs due to the thermal conductivity of different materials. The temperature reaches the highest value in the copper (Cu) pipe, which confirms that it has high thermal conductivity properties. Aluminum (Al) is next, indicating that it has relatively good thermal conductivity. Iron (Fe) and steel (Steel) record the lowest temperature values, indicating that heat transfer is slower than copper and aluminum.

Figure 8 illustrates how the temperature of the heat transfer fluid (HTF) in a solar water heater (SWH) collector with aluminum, copper, iron and steel receiving tubes changes along the length of the collector. The study was conducted for different inlet velocities (0.01 m/s, 0.02 m/s, 0.025 m/s, 0.035 m/s), and the temperature change at each velocity is shown separately. As can be seen from the graph, the temperature of the fluid increases steadily as the collector length increases. At the same time, the rate of temperature increase decreases as the inlet velocity of the fluid increases. At the lowest velocity (0.01 m/s), the HTF reaches the highest temperature, which means that the fluid stays in the tube for a longer time and absorbs more heat. On the contrary, at the highest velocity (0.035 m/s), the temperature of the fluid increases relatively less, since there is not enough time for heat exchange.

These results confirm the importance of choosing the right tube material when designing solar water heater collectors. Materials with high thermal conductivity, such as copper and aluminum, may be the best choice for increasing collector efficiency. However, economic and durability factors should also be considered. As a result, the choice of material should be carefully analyzed based on aspects such as thermal efficiency, cost, and durability to create the most efficient collector system.

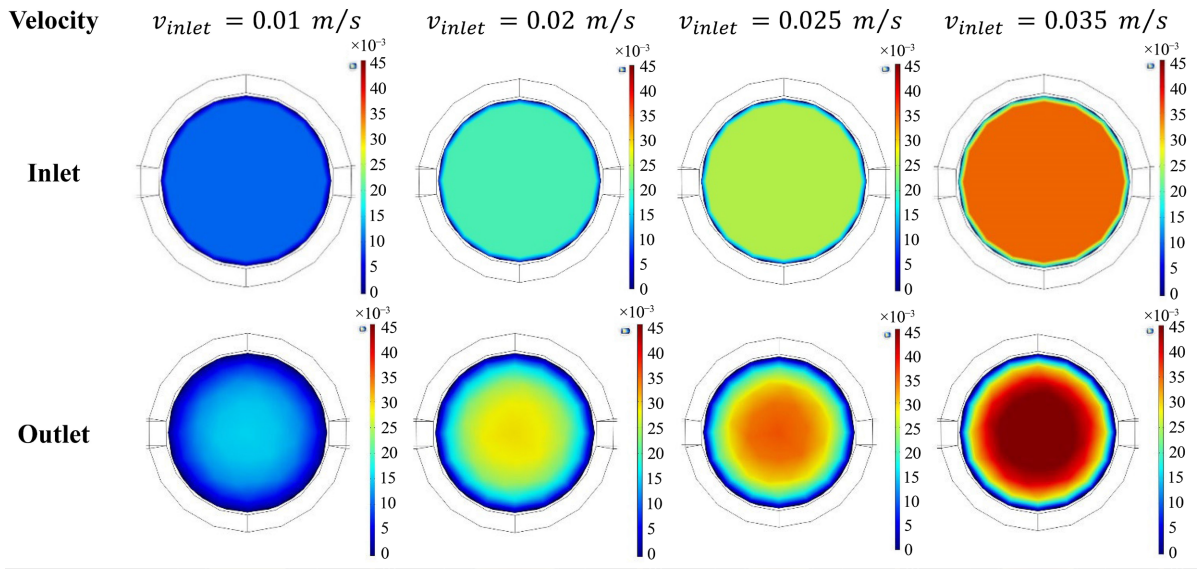

Figure 9. The inlet and outlet water velocities at different flow rates (m/s).

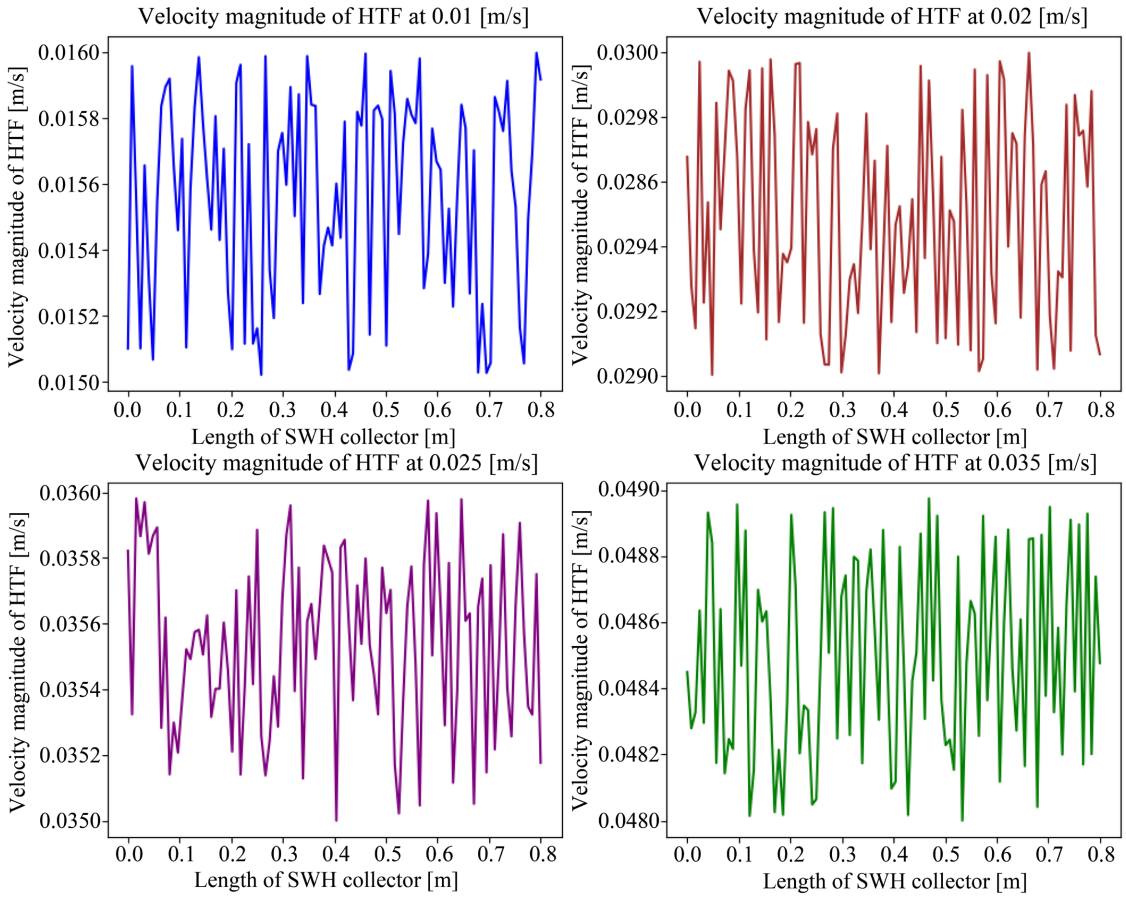

Figure 10. Velocity magnitude of HTF with the length of SWH collector (m/s).

4.3. Impact of the Schematic of the Proposed Collector's Fins

In this section, the effect of the internal spiral pitch variation of the absorber-finned tube on thermal efficiency is numerically investigated. Four different pitch configurations were modeled, and the obtained results were compared with those of a conventional absorber-finned tube. The models considered in this study are illustrated in **Figure 4**. The temperature distribution for different models is presented in **Figure 11**, while the variation of the heat transfer coefficient concerning different inlet velocities is depicted in **Figure 12**. Based on the analysis, the following conclusions can be drawn. First, all proposed models exhibit a higher heat transfer coefficient compared to the conventional collector (Model 1). Second, among the studied models, Model 2 demonstrates the maximum heat transfer coefficient across all investigated inlet velocities. Furthermore, Model 1 exhibits the lowest heat transfer coefficient under all considered inlet velocity conditions.

Figure 12 presents the results of the thermal efficiency analysis of a twisted channel finned tube of a solar water heater collector. The graphs show the effects of different inlet velocities and Model 2 dimensions on the heat transfer process of the collector tube.

Figure 12(a) depicts the temperature variation along the length of the receiving

tube. It can be seen from the graph that as the inlet velocity and fin length increase, the temperature of the heat transfer fluid (HTF) increases. In particular, the maximum temperature is recorded for a fin length of 10 mm and a velocity of 0.01 m/s. Figure 12(b) shows the variation of the convective heat flux along the length of the collector tube. It is seen that a higher inlet velocity (0.02 m/s) increases the heat flux compared to a lower velocity (0.01 m/s), which indicates an increase in heat transfer due to improved fluid movement.

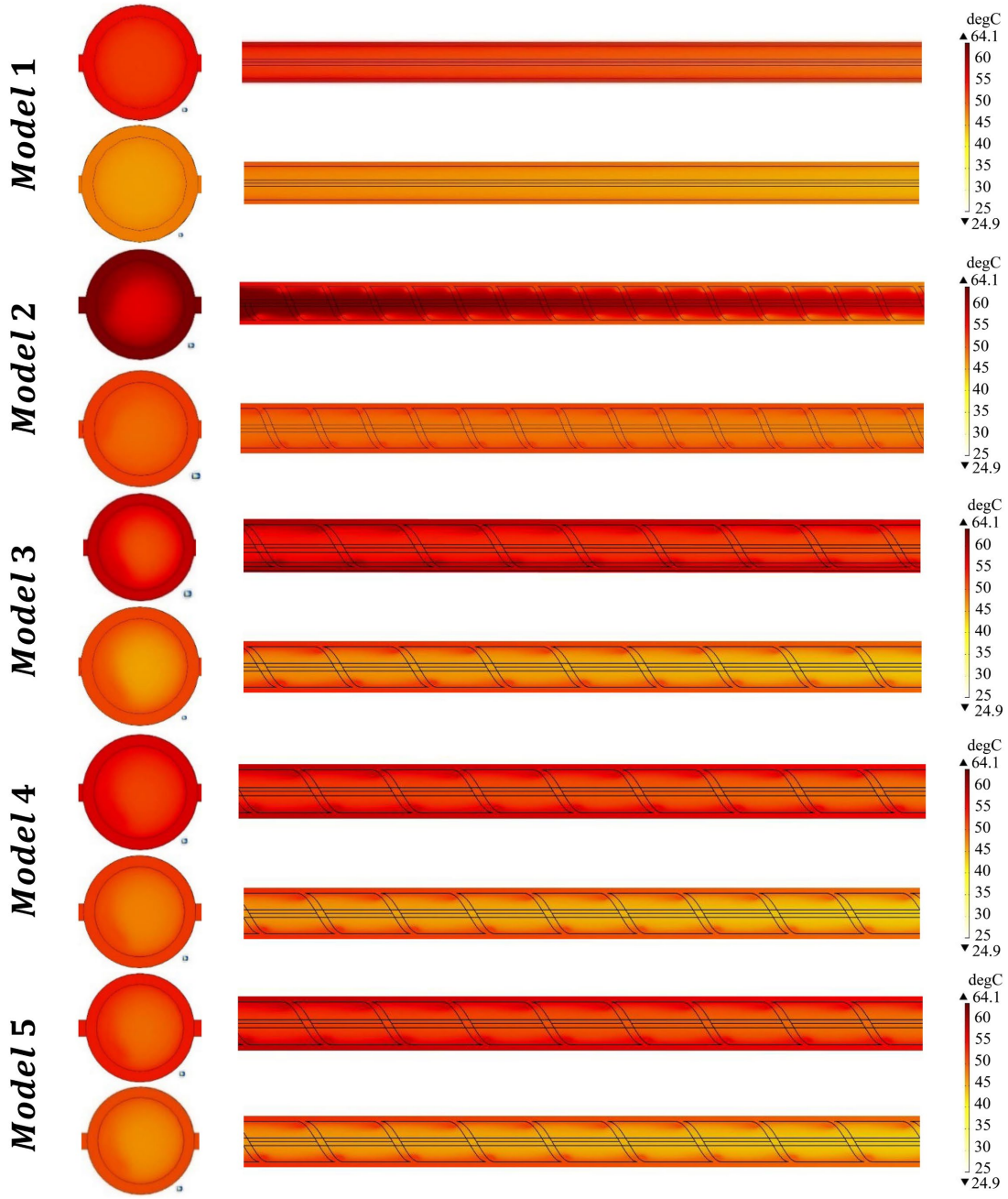

Figure 11. The temperature variation along the surface and the temperature variation of the HTF are presented for 5 different models.

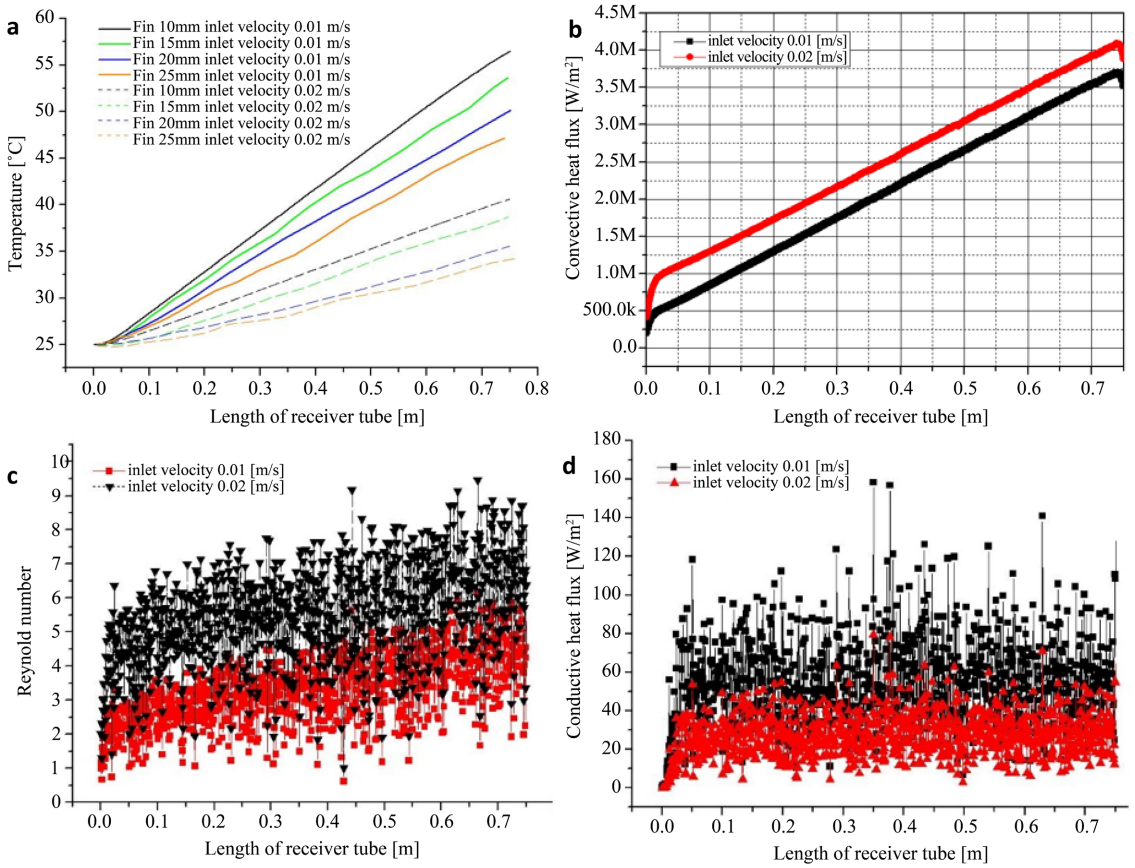

Figure 12. (a) Variation of the temperature along the length of the receiving tube; (b) Variation of the convective heat flux along the length of the collector tube; (c) Variation of Reynolds number along the length of the collector tube; (d) Variation of conductive heat flux along the length of the collector tube.

Figure 12(c) shows the variation of Reynolds number along the length of the collector tube. It can be seen from the graph that at high inlet velocity (0.02 m/s) the Reynolds number shows higher values. An increase in Reynolds number increases the probability of the flow becoming turbulent, which improves heat transfer. Figure 12(d) shows the variation of conductive heat flux along the length of the pipe. The red and black symbols show the results for inlet velocities of 0.01 m/s and 0.02 m/s, respectively. It can be seen from the graph that the conductive heat flux is relatively variable and has sharp changes at different locations.

5. Conclusions

The evaluation of the thermal performance of the solar water heater collector indicates that variations in the absorber finned tube geometry and inlet velocity significantly influence the heat transfer process. The key findings from the analysis are summarized as follows:

Firstly, the temperature distribution along the receiver tube is directly affected by the fin geometry and inlet velocity. A shorter fin pitch combined with higher inlet velocity results in an increased fluid temperature, thereby enhancing heat

transfer efficiency. Secondly, the convective heat flux exhibits a notable increase with higher inlet velocity (0.02 m/s), demonstrating improved thermal exchange within the collector tube. This confirms that enhanced convective heat flux contributes to the overall improvement in the system's heat transfer capability.

Additionally, the analysis of the Reynolds number reveals that a higher inlet velocity leads to an increase in Reynolds number, suggesting a transition towards a more turbulent flow regime. This enhances convective heat transfer and improves the thermal efficiency of the system. In contrast, conductive heat flux variations indicate that thermal distribution within the system is highly dynamic. The observed reduction in conductive heat flux with increased inlet velocity suggests a dominance of convective heat exchange over conduction.

Overall, the results confirm that optimizing the absorber finned tube design and employing a higher inlet velocity significantly improve the thermal efficiency of the solar water heater collector. Notably, the highest heat transfer performance was observed for Model 2, making it the most efficient configuration. In contrast, Model 1 exhibited the lowest heat transfer efficiency. These findings highlight the importance of absorber design optimization and proper selection of flow parameters in enhancing the energy efficiency of solar water heater collectors.

Conflicts of Interest

The authors declare no conflicts of interest regarding the publication of this paper.

References

[1] Delucchi, M.A. and Jacobson, M.Z. (2013) Meeting the World's Energy Needs Entirely with Wind, Water, and Solar Power. *Bulletin of the Atomic Scientists*, **69**, 30-40. https://doi.org/10.1177/0096340213494115

[2] Zaboli, M., Mousavi Ajarostaghi, S.S., Saedodin, S. and Saffari Pour, M. (2021) Thermal Performance Enhancement Using Absorber Tube with Inner Helical Axial Fins in a Parabolic Trough Solar Collector. *Applied Sciences*, **11**, Article 7423. https://doi.org/10.3390/app11167423

[3] Pambudi, N.A., Nanda, I.R. and Saputro, A.D. (2023) The Energy Efficiency of a Modified V-Corrugated Zinc Collector on the Performance of Solar Water Heater (SWH). *Results in Engineering*, **18**, Article ID: 101174. https://doi.org/10.1016/j.rineng.2023.101174

[4] Aramesh, M. and Shabani, B. (2023) Performance Evaluation of an Enhanced Self-Storing Evacuated Tube Solar Collector in Residential Water Heating Application. *Journal of Energy Storage*, **71**, Article ID: 108118. https://doi.org/10.1016/j.est.2023.108118

[5] Rahi, S.M. and AbdulKareem, M.A. (2021) Experimental and Numerical Investigation of the Thermal Performance of Spiral Type Solar Collector. *Journal of Mechanical Engineering Research and Developments*, **44**, 239-250. https://www.researchgate.net/publication/355175758

[6] Yehualashet, K.N., Fatoba, O. and Asfaw, S.M. (2022) Experimental Study and Numerical Analysis of Thermal Performance of Corrugated Plate Solar Collector. *Materials Today*: *Proceedings*, **62**, 2849-2856. https://doi.org/10.1016/j.matpr.2022.02.414

[7] Barbosa, E.G., Araujo, M.E.V.D., Moraes, M.J.D., Martins, M.A., Alves, B.G.X. and

Barbosa, E.G. (2019) Influence of the Absorber Tubes Configuration on the Performance of Low Cost Solar Water Heating Systems. *Journal of Cleaner Production*, **222**, 22-28. https://doi.org/10.1016/j.jclepro.2019.03.020

[8] Syahruddin, A.S., Jalaluddin, J. and Hayat, A. (2021) Performance Analysis of Solar Water Heating System with Plate Collector Integrated PCM Storage. *EPI International Journal of Engineering*, **3**, 143-149. https://doi.org/10.25042/epi-ije.082020.09

[9] Sadhishkumar, S. and Balusamy, T. (2014) Performance Improvement in Solar Water Heating Systems—A Review. *Renewable and Sustainable Energy Reviews*, **37**, 191-198. https://doi.org/10.1016/j.rser.2014.04.072

[10] Farahani, S.D., Farahani, A.D. and Oraki, P. (2021) Improving Thermal Performance of Solar Water Heater Using Phase Change Material and Porous Material. *Heat Transfer Research*, **52**, 69-86. https://doi.org/10.1615/heattransres.2021039550

[11] Alwan, N.T., Majeed, M.H., Khudhur, I.M., Shcheklein, S.E., Ali, O.M., Yaqoob, S.J., *et al.* (2022) Assessment of the Performance of Solar Water Heater: An Experimental and Theoretical Investigation. *International Journal of Low-Carbon Technologies*, **17**, 528-539. https://doi.org/10.1093/ijlct/ctac032

[12] Ramasamy, S. and Balashanmugam, P. (2015) Thermal Performance Analysis of the Solar Water Heater with Circular and Rectangular Absorber Fins. *International Journal of Innovative Science*, *Engineering & Technology*, **2**, 596-603. https://www.ijiset.com

[13] Bhowmik, H. and Amin, R. (2017) Efficiency Improvement of Flat Plate Solar Collector Using Reflector. *Energy Reports*, **3**, 119-123. https://doi.org/10.1016/j.egyr.2017.08.002

[14] Darbari, B. and Rashidi, S. (2021) Thermal Efficiency of Flat Plate Thermosyphon Solar Water Heater with Nanofluids. *Journal of the Taiwan Institute of Chemical Engineers*, **128**, 276-287. https://doi.org/10.1016/j.jtice.2021.06.027

[15] Uzakov, G. and Shamurotova, S. (2024) CFD Analysis for Absorber Tube of a Solar Water Heater Collector. *E3S Web of Conferences*, **498**, Article No. 01013. https://doi.org/10.1051/e3sconf/202449801013

[16] https://www.alibaba.com/premium/solar_heaters_water

[17] Shamuratova, S.M. and Chorieva, S.Y. (2025) Analysis of Flat Solar Water Heating Collector. *Alternative Energy*, **1**, 48-57.

[18] https://socialincome.org/world-poverty-statistics-2023

[19] Farhan, H.A., Nayak, S., Sanjay, and Paswan, M. (2023) Numerical Analysis with Experimental Validation for Thermal Performance of Flat Plate Solar Water Heater Using CuO/Distilled Water Nanofluid in Closed Loop. *Journal of Mechanical Science and Technology*, **37**, 2649-2656. https://doi.org/10.1007/s12206-023-0438-1

Appendix

Nomenclature			
A	Area, [m^2]	ρ	Density, [kg/m^3]
D_1	Diameter of inner the tube, [m]	S	The second Piola-Kirchhoff stress tensor, [Pa]
D_2	Diameter of outer the tube, [m]	T	Absolute temperature, [K]
H	Height of the Fins, [m]	u_{trans}	Velocity vector of translational motion, [m/s]
h_r	Heat transfer coefficient, [W/(m^2·K)]	α	Coefficient of thermal expansion, [1/K]
k_r	Thermal conductivity, [W/(m·K)]	Q	Heat sources, [W/m^3]
L	Length of the tube, [m]	q_r	Heat flux by radiation, [W/m^2]
M	Turbulent Mach number, [nd]	T_{amb}	Ambient temperature [K]
q	Heat flux by conduction, [W/m^2]	T_{in}	Inlet temperature water [K]
C_p	Specific heat capacity, [J/(kg·K)]	T_{out}	Outlet temperature water [K]
Abbreviation			
SWH	Solar water heater	***SWHC***	Solar water heater collector
HTF	Heat transfer fluid	***Lph***	Liter per hour
Exp	Experimental	***LCSHS***	Low-cost solar heating systems
Num	Numerical	***FEM***	Finite element method
PTC	Parabolic trough collector	***in***	Inlet
PCM	Phase change material	***out***	Outlet